An experimental comparison of detector performance for direct and indirect digital radiography systems

Ehsan Samei[a)]
Departments of Radiology, Physics, and Biomedical Engineering, Duke University, DUMC 3302, Durham, North Carolina 27710

Michael J. Flynn
Department of Diagnostic Radiology, Henry Ford Health System, Detroit, Michigan 48202

(Received 10 September 2002; accepted for publication 21 January 2003; published 26 March 2003)

Current flat-panel detectors either directly convert x-ray energy to electronic charge or use indirect conversion with an intermediate optical process. The purpose of this work was to compare direct and indirect detectors in terms of their modulation transfer function (MTF), noise power spectrum (NPS), and detective quantum efficiency (DQE). Measurements were made on three flat-panel detectors, Hologic Direct-Ray DR-1000 (DRC), GE Revolution XQ/i (XQ/i), and Philips Digital Diagnost (DiDi) using the IEC-defined RQA5 (~74 kVp, 21 mm Al) and RQA9 (~120 kVp, 40 mm Al) radiographic techniques. The presampled MTFs of the systems were measured using an edge method [Samei *et al.*, Med. Phys. **25**, 102 (1998)]. The NPS of the systems were determined for a range of exposure levels by two-dimensional (2D) Fourier analysis of uniformly exposed radiographs [Flynn and Samei, Med. Phys. **26**, 1612 (1999)]. The DQEs were assessed from the measured MTF, NPS, exposure, and estimated ideal signal-to-noise ratios. For the direct system, the MTF was found to be significantly higher than that for the indirect systems and very close to an ideal function associated with the detector pixel size. The NPS for the direct system was found to be constant in relation to frequency. For the XQ/i and DRC systems, the DQE results reflected expected differences based on the absorption efficiency of the different detector materials. Using RQA5, the measured DQE values in the diagonal (and axial) direction(s) at spatial frequencies of 0.15 mm^{-1} and 2.5 mm^{-1} were 64% (64%) and 20% (15%) for the XQ/i system, and 38% (38%) and 20% (20%) for the DRC, respectively. The DQE results of the DiDi system were difficult to interpret due to additional preprocessing steps in that system. [DOI: 10.1118/1.1561285]

Key words: image quality, digital radiography, flat panel x-ray detector, resolution, modulation transfer function, MTF, noise, noise power spectrum, NPS, detective quantum efficiency, DQE

I. INTRODUCTION

Digital radiography has gained popularity in many areas of clinical practice. Computed radiography or CR is perhaps the most abundant and common technology today with over 10,000 systems in use worldwide. In the last few years, other digital technologies, most notably the solid state-based flat-panel detector technology, have also gained popularity. Flat-panel systems currently have a higher initial acquisition cost relative to CR. However, they offer potential for better image quality, lower radiation dose, and higher throughput. As the technology becomes more widely available and technological issues are resolved, it is expected that the cost of these systems will go down and clinical utilization will further increase.

All flat-panel detectors consist of an x-ray photon absorption layer coupled to a solid-state array recording layer.[1] In the absorption layer, the energy of the incident x-ray photons is converted to either charge, or to visible light that is subsequently converted to charge in a photodiode layer. In the common solid-state layer, amorphous silicon circuits deposited on a glass plate form an array of thin-film transistors with associated capacitors that collect the produced charge. Each element of the array is responsible for forming a spatial element of the image (i.e., pixel) recorded by the device. After exposure, the charge stored on the capacitors is read line-by-line and element-by-element via associated gate and data lines that turn on the element transistors consecutively. The charge is then amplified, digitized, and stored for subsequent processing and viewing.

There are currently two main types of flat-panel detectors, direct and indirect. The main difference between the two types is the conversion process. For direct detectors, a photoconductive layer, such as amorphous selenium (*a*-Se), converts the x-ray energy to electronic charges that are directed to the collecting pixel capacitors by an electric field.[2,3] For indirect detectors, a scintillation phosphor layer converts the energy of x-ray photons to visible light photons that are subsequently detected by the pixel photodiodes and stored in the form of electronic charge in the capacitors associated with each pixel.[4–6] The phosphor layer may be made from granular phosphor material, such as Gd_2O_2S, or phosphor materials with an oriented structure, such as cesium iodide (CsI).

The relative performance of direct and indirect digital ra-

TABLE I. The imaging systems and their characteristics.

Manufacturer	Detector type	Detector material	Nominal thickness	Pixel pitch (size)	Array size	Imaging area
Direct Radiography Corp. (Hologic) DR-1000 (DRC)	Direct	*a*-Selenium	0.500 mm	0.139 mm	2560×3072 2 subpanels	35×43 cm^2
General Electric Co, Revolution XQ/i (XQ/i)	Indirect	CsI (Tl)	[a]	0.2 mm	2048×2048 single panel	41×41 cm^2
Philips Medical Systems, Digital Diagnost (DiDi)	Indirect	CsI (Tl)	0.500 mm	0.143 mm	3001×3001 4 subpanels	43×43 cm^2

[a]Not disclosed.

diographic systems influences their clinical effectiveness. Therefore, there is a need to assess and compare the performance of these systems. The performance of some direct and indirect detectors has been previously studied, focusing on the evaluation of single systems.[7–10] However, there are significant methodological differences between these studies that make it difficult to directly compare their results. The purpose of this work was to assess the performance of three commercial, full-sized, direct and indirect flat-panel digital radiographic systems. The characteristics considered were the modulation transfer function (MTF), the noise power spectrum (NPS), and the detective quantum efficiency (DQE). The three systems were evaluated using identical methods so that direct comparisons could be made. Some of the preliminary results of this investigation were previously reported in a conference proceedings.[11] This paper reports the complete findings of this investigation and supersedes the proceedings article.

II. MATERIALS AND METHODS

A. Imaging systems

The physical characteristics of the three systems tested are tabulated in Table I. All systems were commercial-grade and had full-sized recording fields suitable for standard adult radiographic applications. The XQ/i and DiDi systems were installed in the Radiology Department at Duke University. The DRC system was installed at the manufacturer's laboratory, but was otherwise evaluated by the same methods and investigators. All three systems were FDA approved for clinical use. The systems were tested with configurations and settings identical to those used for clinical procedures with the exception that the antiscatter grids were removed. The DRC system was tested with a carbon-fiber barrier covering the detector. The XQ/i system was tested with the detector barrier containing the grid removed, but the system still included an ionization chamber and the detector seal. The DiDi system was tested with the detector barrier in place. Before initiating the measurements, all three systems were calibrated without grid according to manufacturers' guidelines. For all data acquisitions, the images were transferred as raw, unprocessed data to our research computers via magneto-optical disks (MODs) or CD-R media. For the DRC and the XQ/i, the manufacturers verified that only basic uniformity and offset corrections were applied to the raw data. For the DiDi, some additional preprocessing corrections were applied, as described in the Discussion.

B. X-ray techniques

The systems were evaluated using two standard beam qualities, RQA5 and RQA9 described by an International Electrotechnical Commission (IEC) standard.[12] The IEC standard defines the various RQA techniques by the added filtration and the half-value-layer (HVL) of the beam. For each of the systems tested, the RQA5 technique was set up by placing 21 mm of aluminum (1100 alloy) in the beam. The kVp was then adjusted to obtain an HVL of 7.1±0.1 mm. The RQA9 technique was obtained by placing a 40 mm aluminum filter in the beam and adjusting the kVp to obtain an HVL of 11.5±0.1 mm. Table II lists the kVp settings

TABLE II. The standard x-ray beam characteristics used to evaluate detector performance.

Detector	Technique	Filtration (mm Al)	HVL (mm Al)	kVp	Intrinsic filtration: 1.48 mm Pyrex, 3.0 mm Oil, plus	Ideal SNR^2, Energy-weighted (#/mm^2 mR)	Ideal SNR^2, counting (#/mm^2 mR)	Percent difference
DRC	RQA5	21	7.1	74	2.45 mm Al	255,731	262,773	2.7%
	RQA9	40	11.5	123		257,729	271,197	5.1%
XQ/i	RQA5	21	7.1	74	1.90 mm Al	255,855	263,180	2.8%
	RQA9	40	11.5	120		259,531	272,738	5.0%
DiDi	RQA5	21	7.1	78	2.25 mm Al	259,400	267,249	3.0%
	RQA9	40	11.5	120		259,527	272,687	4.9%

required to obtain the desired HVLs. All kVps were verified to be within 2 kVp of the desired values using a noninvasive method.

All measurements used x-ray sources with high-frequency generators, a small focal spot, and a source-to-image distance (SID) greater than 180 cm. There was a minimum of one minute delay between acquisitions to minimize the contribution of any potential lag signal in the acquired data. For each image acquisition, a calibrated ion-chamber ($10\times5-6$ ionization chamber, 1015 x-ray monitor, Radcal Corporation, Monrovia, CA) was positioned half way between the tube and the receptor. The chamber was positioned so that it projected over the corner of the detector. Care was exercised to assure the entire collection volume of the chamber was within the beam. For each acquisition, the exact exposure to the detector was calculated using the inverse square of relative distances and relative signal variations across the detector area [see Sec. II E (h) below].

C. System response and linearity

Linearity of the systems was verified within the tested exposure range. At each beam quality, multiple uniform images were acquired using different exposures. The averages of the pixel values within 80% of the image were computed and the results plotted as a function of exposure (Fig. 1). All three systems demonstrated excellent linearity ($R^2>0.9996$). The pixel values in the DRC and XQ/i systems exhibited a linear relationship with exposure, while those for the DiDi system were proportional to the logarithm of exposure. The relationships were used to linearize the image data with respect to exposure with zero offset, an important requirement of linear system analysis.

D. Modulation transfer function (MTF)

The presampled modulation transfer functions of the systems were measured using an established edge method.[13] For this study, a new edge test device was constructed (Fig. 2). The device consisted of a 5×5 cm^2 square $Pt_{90\%}-Ir_{10\%}$ foil with a 0.1 mm thickness and 99.9% purity. The foil was laminated between two, 1 mm thick slabs of acrylic. All four edges of the laminate were polished to submicron smoothness. The edge device had a measured transmission of 44.9% and 33.4% for the RQA9 and the RQA5 techniques, respectively.

For image acquisition, the device was placed perpendicular to the incident x-ray beam at the center of the detector with a 5–10 degree angle between the detector array and the edges of the device. It was verified that moving the edge device by up to ±2.5 cm off-center would not affect the measured MTF, as independently verified by others.[14] Images were then acquired using RQA5 and RQA9 techniques (as described above) with an incident exposure at approximately 2/3 of the saturation exposure for each imaging system. The exposures used were 6.2 and 5.9 mR, 6.1 and 5.4 mR, and 4.4 and 4.0 mR at RQA5 and RQA9 techniques for the DRC, XQ/i, and DiDi systems, respectively. The image data were processed to deduce the MTF using a recently developed MTF analysis program. This program used methods similar to those described in a prior report,[13] with only minor differences. The major elements of the MTF analysis program were as follows:

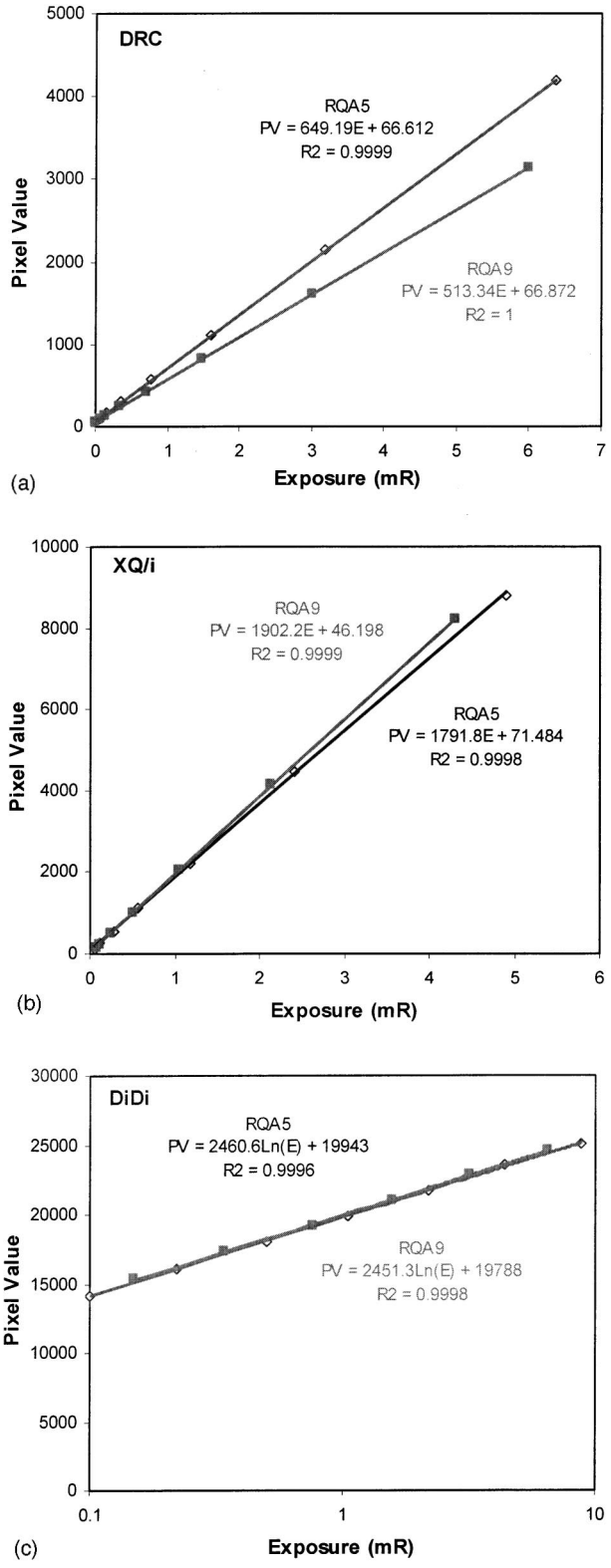

FIG. 1. The relationship between the pixel value and exposure for the DRC (a), XQ/i (b), and DiDi (c) systems at the RQA5 and RQA9 techniques.

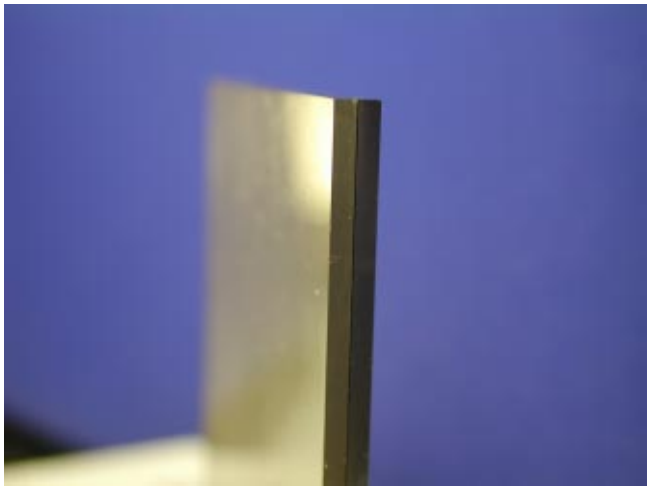

FIG. 2. The cross section of the edge test device used for MTF measurements.

(a) **ROI extraction**: From the linearized image data, a central region of interest (ROI) containing the central part of a vertical or a horizontal edge transition was extracted.
(b) **Angle determination**: The exact angle of the edge line in the ROI was determined by a least square fit to the edge transition data.
(c) **ESF computation**: The image data within the ROI were projected along the edge line to obtain the edge spread function (ESF) relating the pixel value to the perpendicular distance from the edge. In the projection, the data values within ± 2.0 mm of the edge were rebinned into 0.1 pixel spacing. The raw ESF data that were not near the edge were smoothed using a moving polynomial fit (Savitzky–Golay method).[15]
(d) **LSF computation**: The ESF was differentiated to obtain the line spread function (LSF). A Hann (i.e., Hanning) window function[16] with a window width of 4 mm was then applied to the LSF data in order to reduce the influence of small differences in the LSF tails and to condition the data for spectral estimation.[13]
(e) **MTF computation**: The MTF, in the direction perpendicular to the original edge line, was computed by performing a fast Fourier transformation (FFT) of the LSF and normalizing its value to unity at zero spatial frequency.

For detectors with multiple subpanels (i.e, DRC and DiDi), the MTF was measured at the center of each subpanel separately, and the results were averaged to obtain the detector's MTF. The correlation coefficient of the MTFs from any two subpanels was also assessed. The value of the correlation coefficient for the DRC system, or the minimum for the six subpanel pairs for the DiDi system, was indicated as the maximum variability of MTF among subpanels of the detector.

E. Noise power spectrum (NPS)

The noise power spectra of the systems were measured from uniform images using a two-dimensional Fourier analysis method.[17] Uniform images were acquired using RQA5 and RQA9 beam qualities at multiple exposure levels. For each acquisition, the precise exposure to the detector was measured using a calibrated ion chamber, as described above. The major elements of the NPS analysis were as follows.

(a) **ROI definition**: The image data, excluding the edges, was divided into ~100 ROIs, each 128×128 pixels in size.
(b) **Removal of medium-scale nonuniformities**: A two-dimensional second-order polynomial was fit to the data within each ROI and the fit was subtracted from the data to remove background trends.
(c) **Noise conversion**: The noise within each ROI was converted to relative noise by dividing the data by their mean value.
(d) **ROI NPS computation**: A Hamming filter was applied to the data followed by a fast Fourier transformation (FFT) to obtain each ROI's NPS.
(e) **Removal of large-scale nonuniformities**: The NPS from each ROI was scaled by its mean value relative to that of the upper-left reference ROI. In doing so, the influence of large-scale nonuniformities, such as the heel effect, on the overall resultant NPS was eliminated.
(f) **2D NPS computation**: The scaled NPS for all the ROIs were averaged to obtain the overall two-dimensional NPS.
(g) **1D NPS computation**: The one-dimensional (1D) NPS in the horizontal, vertical, and 45° diagonal directions were obtained by averaging the directional frequency bands in the 2D NPS, central axes ± 5 horizontal, vertical, or diagonal lines.
(h) **Exposure determination**: The effective exposure to the detector was determined from the measured exposures corrected by the inverse-square law and by the average signal difference between the image area surrounding the ion-chamber and the upper-left reference ROI. The exposure reported with the computed NPS was the detector exposure at the reference upper-left ROI of the image. As all ROI NPS were scaled relative to the reference ROI [step (e)], the computed average NPS [step (f)] was associated with the proper exposure.

For detectors with multiple subpanels (i.e., DRC and DiDi), the NPS was measured within the central area of each subpanel separately, and the results were averaged to obtain the detector's NPS. The correlation coefficient of the NPS from any two subpanels was also assessed. The value of the correlation coefficient for the DRC system, or the minimum

for the six subpanel pairs for the DiDi system, was indicated as the maximum variability of noise among subpanels of the detector.

F. Detective quantum efficiency (DQE)

The detective quantum efficiencies of the systems were deduced from the measured MTF, the measured NPS, the exposure, X, and estimated values for the ideal SNR^2 per mR, q, as described in previous publications:[17,18]

$$\mathrm{DQE}(f)=\frac{G\times \mathrm{MTF}^2(f)}{q\times X\times \mathrm{NPS}(f)}. \tag{1}$$

In this equation, G is a gain factor that is equal to unity because of the data linearity and the NPS normalization. The q values were calculated using an x-ray spectrum computed by an x-ray modeling and simulation program (xSpect, Henry Ford Health System). The program is based on a semiempirical computational model for x-ray simulation and accounts for various attenuation processes in the image formation.[17] For each system, the spectra were first adjusted to agree with the HVL measurements by slightly adjusting the assumed intrinsic filtration. The estimated intrinsic filtrations associated with each system were then used in the simulation program along with the added filtration and measured kVp values to simulate a spectrum incident on the detector. The q values were estimated by assuming that an ideal detector behaves as a perfect energy integrator of the x-ray or alternatively as a photon counter as described in a previous publication.[18]

The calculated q values for all three systems at RQA5 and RQA9 are reported in Table II. The variation among systems is due to differences in the estimated intrinsic filtrations and the measured kVps used to adjust the beam quality. For a given system and a beam quality, the difference between the two types of q values range between 3% to 5%, depending on the kVp. For higher kVp spectra with a more nonsymmetrical shape, there is more difference between the results of energy-weighted and counting q values. Based on our previous work,[17,18] we used an energy-weighted q for the DQE computations. The reported DQEs, however, may be adjusted by the factors tabulated in Table II, if DQE estimates referenced to a ''counting'' ideal detector are sought.[19]

The DQEs of the systems were computed for 1D spatial frequencies in the horizontal, vertical, and diagonal directions. The 1D NPS values used for the three directions were derived from the 2D NPS as described above. Since the MTF was experimentally measured only in the horizontal and vertical directions, the diagonal MTF was estimated from the results for the two axial directions. For the indirect systems, an isotropic presampled MTF was assumed[20] and the diagonal MTF estimated as the average of the vertical and horizontal MTFs. For the direct system, since the sampling aperture plays a determinant role in defining the MTF, the diagonal presampled MTF was estimated from the average of axial MTFs using an aperture scaling function,

$$\mathrm{MTF}_{\mathrm{diag}}(f)=\frac{\mathrm{sinc}^2_{\pi}(pf/\sqrt{2})}{\mathrm{sinc}_{\pi}(pf)}\mathrm{MTF}_{\mathrm{ax}}(f), \tag{2}$$

where p is the pixel size in mm, and f is the spatial frequency in mm^{-1}. The numerator represents the Fourier representation of the pixel aperture in the diagonal direction (i.e., a triangular sampling function), and the denominator term represents the Fourier representation of the pixel aperture in the axial direction (i.e., a square sampling function). Using this equation, $\mathrm{MTF}_{\mathrm{diag}}$ is slightly higher than $\mathrm{MTF}_{\mathrm{ax}}$ by 0.001, 0.014, and 0.057 at $0.5f_N$, f_N, and $1.5f_N$, where f_N is the Nyquist frequency.

III. RESULTS

Figure 3 illustrates the MTF results for the three systems in the horizontal and vertical directions for the RQA5 technique. For comparison, the ''ideal'' MTFs for each system are also shown in reference to the best possible MTF dictated by the aperture size of the detector elements. Comparing the three systems, the MTF for the DRC system was very close to the ideal sinc, whereas those for the indirect systems were notably lower than their corresponding ideal sinc functions. It should be noted that the MTF for the DiDi system was enhanced by preprocessing of raw image data in that system (see description in Discussion). The horizontal and vertical MTFs were nearly identical for all three systems. The vertical MTFs were slightly higher than the horizontal ones, which may be attributed to the spatial structures of the TFT elements. The MTFs were also nearly identical for the RQA9 technique (not shown). Slight technique dependencies were observed in the $0.1-1\ \mathrm{mm}^{-1}$ frequency range for the XQ/i and DiDi systems for which the RQA9 MTFs were slightly lower than the RQA5 results (maximum difference$=0.045$ at $0.6\ \mathrm{mm}^{-1}$). This difference may be attributed to secondary radiation form the edge device at high x-ray energies. In detectors that consisted of multiple subpanels, the resolution characteristics for the subpanels were very similar. The correlation coefficients of the MTFs of the upper and lower subpanels of the DRC system at various exposure levels were greater than 0.998. The correlation coefficients of the MTFs of the four subpanels of the DiDi system were greater than 0.997.

Figure 4 illustrates the 2D NPS for the three systems using an RQA5 technique with 1–2 mR exposure. For the detectors with multiple subpanels, the spectrum is shown for each subpanel. For the DRC system [Fig. 4(a)], the NPS was relatively uniform across all frequencies. In comparison, the two indirect detectors exhibited a sharp drop in the NPS at high frequencies. The XQ/i system exhibited elevated noise in the horizontal direction, possibly due to slight structured noise patterns in that direction. The NPS for the DiDi system showed marked depression on the horizontal and vertical axes of the 2D spectra due to preprocessing (see Discussion). Very similar behaviors were observed at other exposures and at RQA9 beam quality.

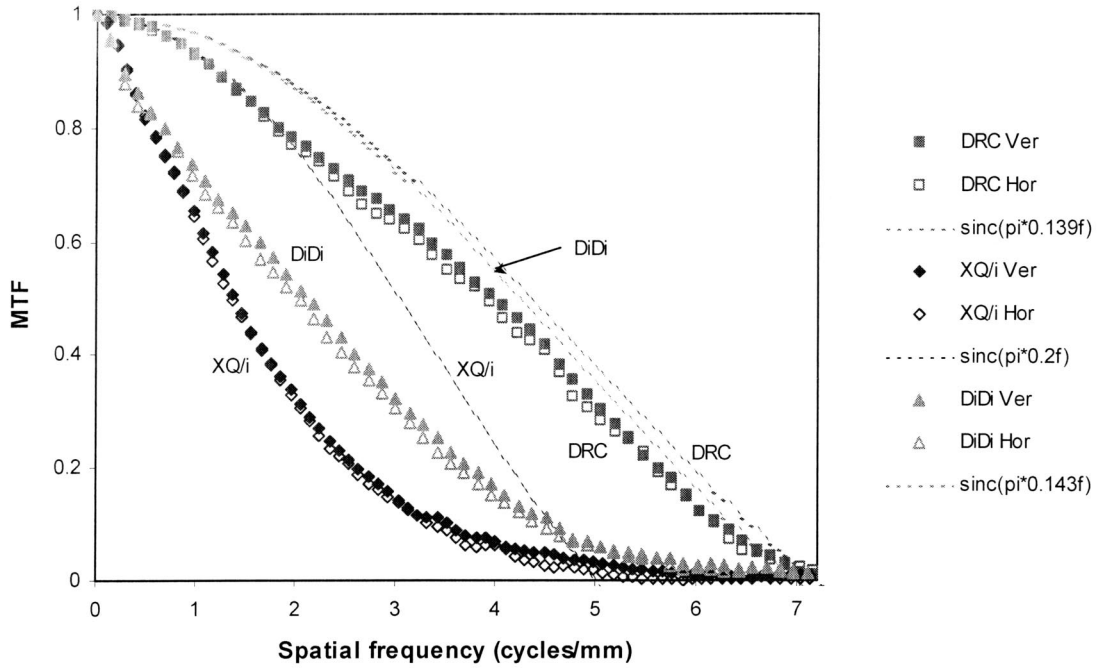

FIG. 3. The measured MTFs for the DRC, XQ/i, and DiDi imaging systems. The increased MTF of the DiDi system at mid frequencies is partly due to image preprocessed applied to raw image data in that system.

Figure 5 illustrates the NPS in the vertical, horizontal, and 45° diagonal directions for the three systems at various exposures using the RQA5 and RQA9 techniques. As similarly illustrated in Fig. 4, the NPS for the DRC direct detector were relatively flat and similar to that for white noise. The indirect systems [Figs. 5(c), 5(d), 5(e), and 5(f)] exhibited significant reduction at high spatial frequencies. For the DiDi system, the NPS decreased with increased exposure at a less than the expected rate (<1/exposure). Additionally, the DiDi system demonstrated increased noise in the vertical direction at high exposures for frequencies above 2 mm^{-1}. The differences in the noise characteristics of subpanels in multipanel detectors are illustrated in Fig. 6 by plotting the minimum correlation coefficient as a function of exposure. Poor correlation is evident for the DiDi system at high exposures.

Figure 7 illustrates the axial and the diagonal DQE for the XQ/i and DRC systems at three exposures using the RQA5 and RQA9 techniques. The DQEs for the DiDi systems are not reported as such results were affected by nonlinear preprocessing operations applied to the ''raw'' image data, indicated above and discussed in the Discussion. The DRC system exhibited a nearly inverse-linear relationship with spatial frequency for both RQA5 and RQA9 techniques. The results from the two subpanels were averaged, since the correlation coefficients of the DQE of the upper and lower subpanels were greater than 0.987. Compared to the DRC, the DQE of the XQ/i system was notably higher at lower frequencies but dropped more rapidly at higher spatial frequencies. For both systems, the DQE at mid to high spatial frequencies were higher in the diagonal direction than the axial direction. The differences were more notable for the XQ/i system. Furthermore, the DQE of the XQ/i system exhibits some exposure dependency with lower DQEs at higher exposures. For these two systems, the magnitudes of the DQEs at near zero frequencies were consistent with expectation based on the absorption efficiencies for the detective materials. The difference between the RQA5 and RQA9 results was as expected in that the higher energy photons of the RQA9 technique are less efficiently absorbed by the detector material. Furthermore, as the *a*-Se layer in the DRC system has a lower atomic number than the CsI layer in the XQ/i system, the relative reduction in DQE with increased beam energy was more substantial for the DRC system.

IV. DISCUSSION

Digital radiography using solid-state detectors is emerging as a viable technology for acquiring digital x-ray images. Many manufacturers now offer medical imaging systems based on this technology. However, there are important differences in the particular implementations of the technology, most notably in the use of photoconductor-based (i.e., direct) or phosphor-based approaches (i.e., indirect) for x-ray detection. Ultimately, the utility of these approaches should be examined by clinical trials. In the absence of clinical trial results, the key physical attributes of these systems can be evaluated experimentally and used to predict the clinical efficacy of various implementations of the technology. In this study, we have compared the resolution (MTF), noise (NPS), and signal-to-noise (DQE) characteristics of one direct-type and two indirect-type digital radiographic systems.

The MTFs determined for the three systems examined indicated that the MTF was notably higher for the direct

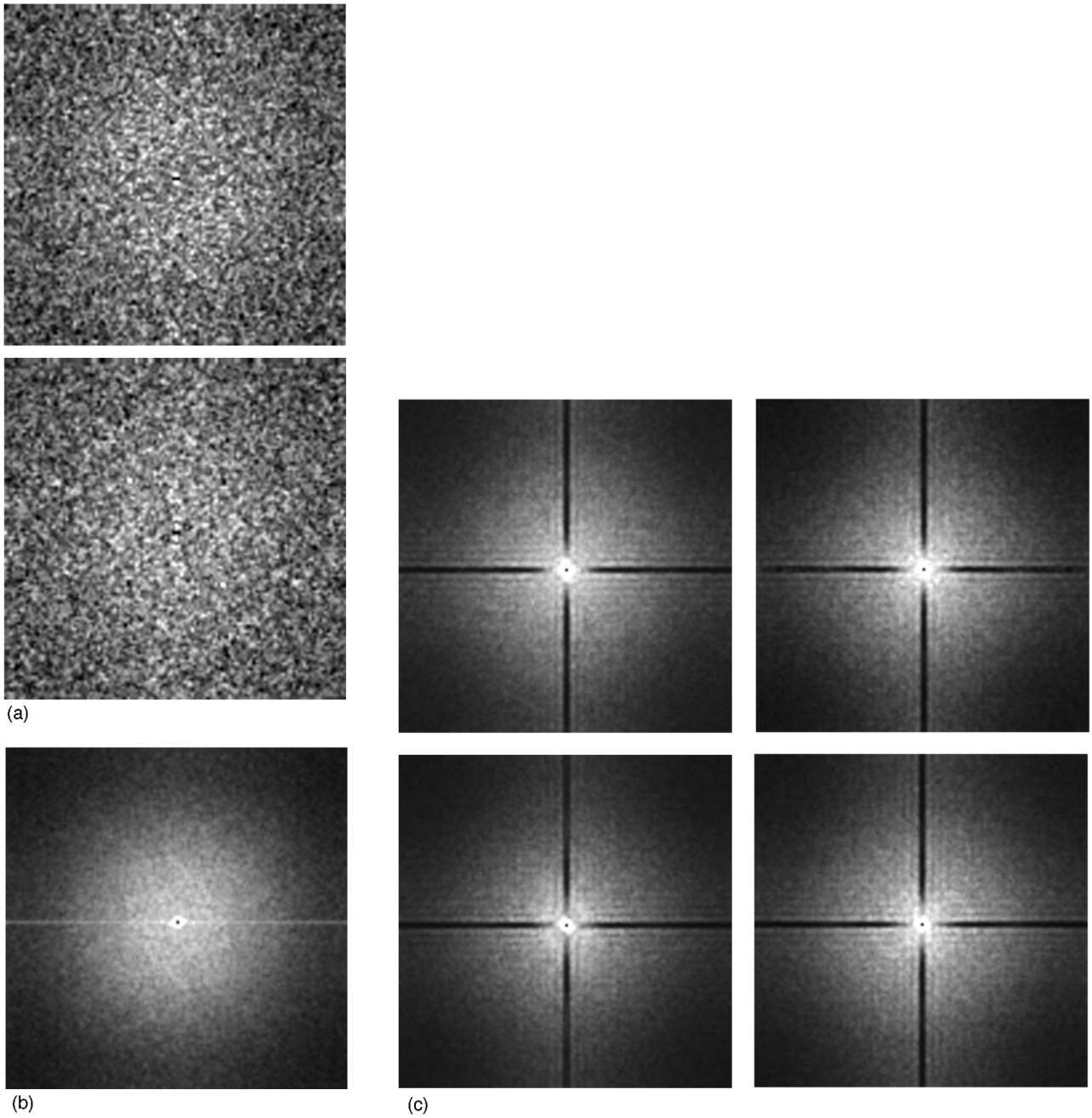

FIG. 4. The measured 2D NPS for the two subpanels of the DRC system at 1.74 mR (a), for the XQ/i system at 1.19 mR (b), and for the four subpanels of the DiDi system at 1.23 mR (c). The data were acquired with the RQA5 beam quality. A consistent brightness and contrast setting was used for all spectra.

detector system. Table III compares the MTF results. For the direct detection DRC detector, the charge is collected with little spread and thus good resolution is expected relative to the indirect detection systems where light scattering causes blur. The resolution response of the XQ/i system was seen to be similar to that of CR systems. The other indirect system tested, the DiDi system, exhibited superior MTF response compared to XQ/i. However, because of the preprocessing steps applied to the raw image data in this system (described below), the results cannot be considered as a true representation of the intrinsic resolution characteristics of the system.

Table IV compares the DQE results. In general, higher DQE translates into better image SNR or reduced patient dose at comparable SNR. At lower frequencies, the DQE for the indirect XQ/i system was noticeably higher than the direct DRC's due to the good absorption characteristics of the detection layer. The DQE for this system, however, decreased more rapidly with frequency compared to that of the DRC. Also notable was the different limiting frequencies for these two systems, $2.5\,\mathrm{mm}^{-1}$ and $3.6\,\mathrm{mm}^{-1}$, respectively. The DQE responses in the diagonal direction crossed at a frequency of about $2.5\,\mathrm{mm}^{-1}$ for RQA5 and at $2.9\,\mathrm{mm}^{-1}$ for RQA9 (Fig. 7). The corresponding crossover point in the averaged axial direction for the RQA5 technique was $2.3\,\mathrm{mm}^{-1}$. The axial DQEs did not cross for RQA9. At frequencies below these crossover points, the XQ/i system per-

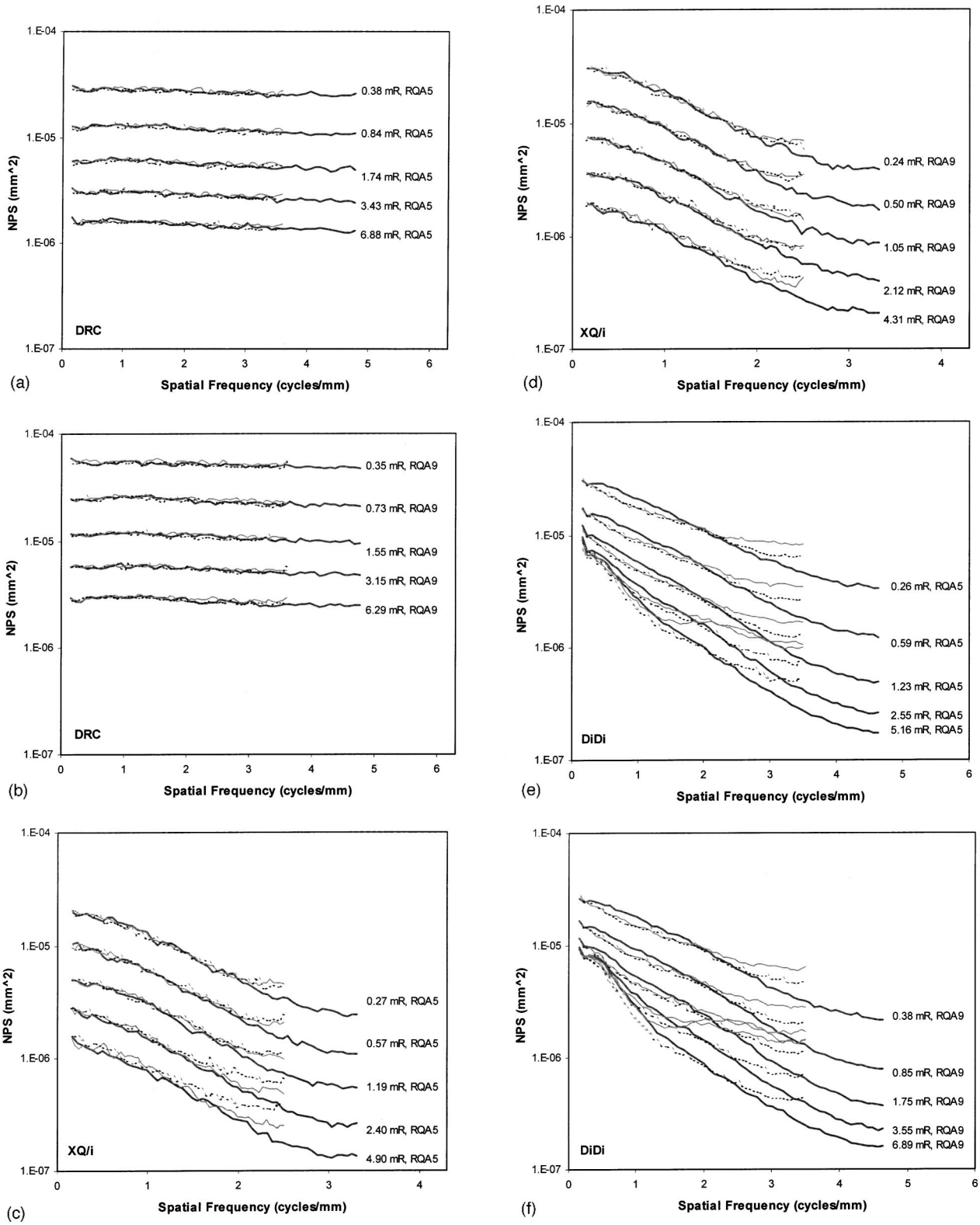

FIG. 5. The measured NPS in the vertical (—), horizontal (- - -), and 45° diagonal (——) directions with the RQA5 and RQA9 beam qualities for the DRC system (a) and (b), the XQ/i system (c) and (d), and the DiDi system (e) and (f), respectively.

formed better while at frequencies above these crossovers, the DRC system was superior.

We are not aware of prior reports on the performance of the DiDi system. Our results were notable with respect to the differences between the DiDi system and the other indirect system evaluated (i.e., XQ/i). Upon a retrospective inquiry, the manufacturer indicated the raw image data from that system were preprocessed. In particular, two preprocessing steps

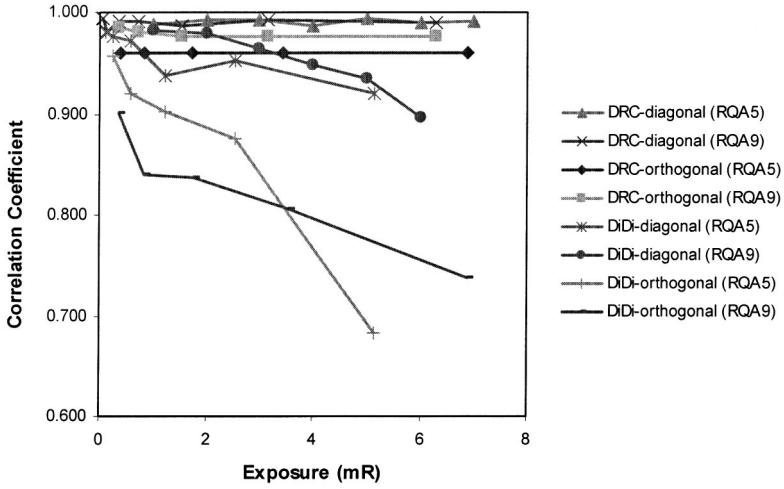

FIG. 6. The correlation coefficient of one-dimensional NPS estimates from multiple subpanels of multipanel detectors evaluated.

are applied to all raw images from that system: (a) An unsharp-mask filter is applied to the linearly scaled data with a kernel size of 3×3 pixels. The enhancement factor applied increases from 0 to 1.5 linearly with exposure up to an exposure of 0.277 mR, beyond which the factor is constant at 1.5. (b) Destriping filters are applied with kernels of 81×9 and 9×81 pixels in the horizontal and vertical directions, presumably to reduce the detector structured noise. Amplitudes of these filters change nonlinearly with signal level and variance. Ideally, the performance of this system should be evaluated using image data prior to these preprocessing operations. However, in the absence of access to such data,

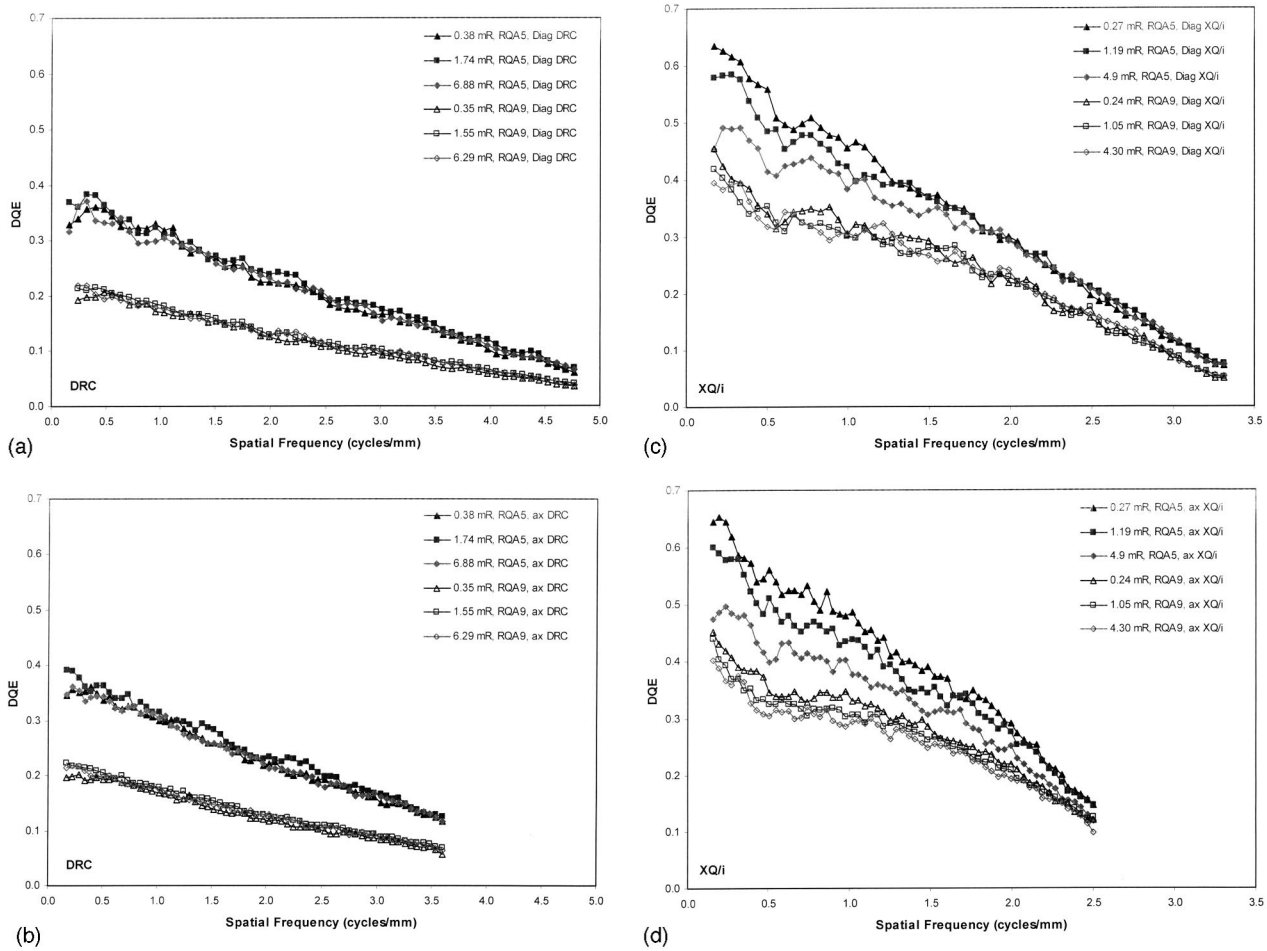

FIG. 7. The DQE at RQA5 and RQA9 beam qualities for the DRC system in the diagonal (a) and axial (b) directions, and for the XQ/i system in the diagonal (c) and axial (d) directions.

TABLE III. The MTF results (obtained from the RQA5 and RQA9 techniques) are summarized by tabulating the average of the response in the horizontal and vertical directions. For comparison, the results for a typical CR system are also shown.

MTF	DRC	XQ/i	DiDi[a]	CR[b]
0.2	5.6 mm^{-1}	2.6 mm^{-1}	3.7 mm^{-1}	2.4 mm^{-1}
0.1	6.2 mm^{-1}	3.5 mm^{-1}	4.5 mm^{-1}	3.4 mm^{-1}

[a]Reported values include the effects of preprocessing applied to raw image data from this system.
[b]Fuji, FCR-9501-HQ, ST-Va, 0.1 mm pixel, from Samei and Flynn (Ref. 18).

carefully performed image quality assessments can be valid[9] if viewed in light of the particular characteristics of the image preprocessing.

For the DiDi system, the MTF data were acquired at an exposure level at which the detector exposure at both sides of the edge fell within the region where the applied unsharp mask filtering coefficients were constant. Thus, as far as this filtering operation, the MTF analysis did not violate the linearity requirement for a linear system analysis. However, the destriping filters still applied. Furthermore, for the NPS evaluations, the exposures were also beyond the constancy threshold of the unsharp mask filtering. Thus, as far as this filtering process is concerned, the MTF and NPS are affected similarly, and the DQE remains unaffected. The destriping filters clearly impact the NPS results on the axes of the 2D NPS. This effect can be minimized by extracting the 1D NPS from a diagonal band through the 2D NPS, as done for this report. However, the MTF is still affected, thus impacting the resulting DQE. Thus, this study does not report the DQE of the DiDi system. Furthermore, any direct comparison of the MTF and NPS of this system with those from the other two systems may only be made taking into account the above preprocessing operations.

In this study, for the first time, we examined the noise and DQE performance of radiographic systems in the 45° diagonal direction. The diagonal response enables the examination of a system's response beyond the cutoff frequency determined by the pixel spacing in the axial direction while at the same time reduces the contribution of noise aliasing to the DQE estimate. This is illustrated in Fig. 5, which shows a decreased NPS at high frequencies for the diagonal direction relative to the axial directions. Figure 8 illustrates the corresponding increase in the DQE at high frequencies in the diagonal direction (0.049 at the Nyquist frequency of 2.5 mm^{-1} for RQA5, 0.27 mR) for the XQ/i system. Similar examination of the DRC system response [Figs. 7(a) and 7(b)] reveals a relatively smaller difference between the axial and diagonal DQEs (0.011 at the Nyquist frequency of 3.6 mm^{-1} for RQA5, 0.38 mR). As is seen for the NPS results (Fig. 5), the wide bandwidth of the noise spectrum for this system results in similar aliasing in all directions when sampled by the square pixel aperture. Also shown in Fig. 8, radial DQE, calculated from the radically averaged 2D NPS

TABLE IV. The DQE at specific spatial frequencies for the RQA5 and RQA9 at approximately 0.3 mR detector exposure. For comparison, the results for a typical CR system are also shown.

	DRC		XQ/i		CR[a]
	RQA5 technique				70 kVp, 19 mm Al
Frequency (mm^{-1})	Diagonal	Axial	Diagonal	Axial	Axial
0.15	0.38	0.38	0.64	0.64	0.30
0.5	0.36	0.36	0.58	0.58	0.26
1.0	0.32	0.32	0.47	0.47	0.20
1.5	0.27	0.27	0.37	0.37	0.15
2.0	0.23	0.23	0.30	0.30	0.10
2.5	0.20	0.20	0.20	0.15	0.07
3.0	0.17	0.15	0.12		0.04
3.5	0.13	0.12			0.02
4.0	0.10				0.02
4.5	0.08				0.01
	RQA9 technique				115 kVp, 19 mm Al
	Diagonal	Axial	Diagonal	Axial	Axial
0.15	0.22	0.22	0.45	0.45	0.23
0.5	0.21	0.21	0.35	0.35	0.19
1.0	0.18	0.18	0.31	0.31	0.15
1.5	0.16	0.16	0.29	0.29	0.12
2.0	0.13	0.13	0.22	0.22	0.08
2.5	0.11	0.11	0.15	0.12	0.05
3.0	0.09	0.08	0.09		0.03
3.5	0.07	0.06			0.02
4.0	0.06				0.01
4.5	0.05				0.01

[a]Fuji, FCR-9501-HQ, ST-Va, 0.1 mm pixel, from Samei and Flynn (Ref. 18).

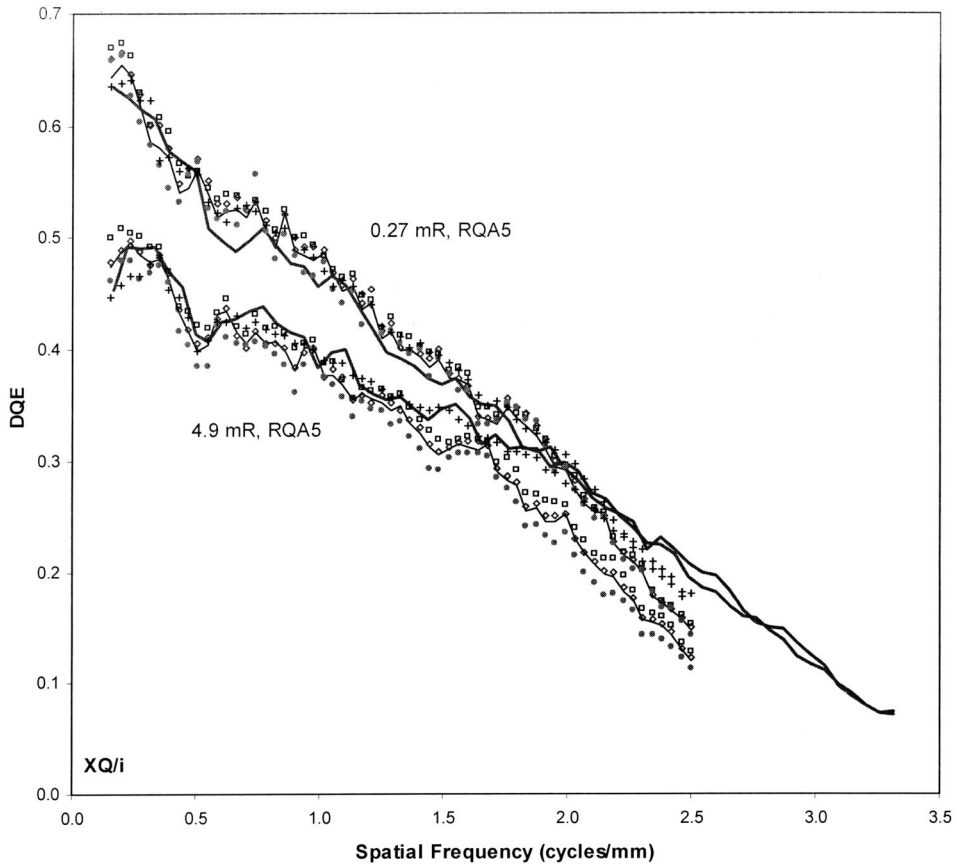

FIG. 8. Diagonal, axial, and radial DQE for RQA5 beam quality at two exposures for the XQ/i system. The results are from one-dimensional NPS derived from 2D NPS by radial averaging (+), averaging 0.28 mm^{-1} wide diagonal bands (——), averaging 0.39 mm^{-1} wide axial bands (- - -), averaging 0.55 mm^{-1} wide axial bands excluding central axes (□), averaging 0.39 mm^{-1} wide axial bands excluding central axes (◇), and averaging 0.23 mm^{-1} wide axial bands excluding central axes (●).

and the average of the axial MTFs, exhibit a DQE at high frequencies intermediary to the axial and diagonal DQEs, averaging the contribution of noise aliasing in the axial and diagonal directions in the estimate of the DQE.

Our results for the DRC system are consistent with prior reports.[2,21] While we report DQE only to a minimum spatial frequency of 0.15 mm^{-1}, the zero frequency response was estimated by extrapolation to be 39% for RQA5 and 22% for RQA9. In comparison, Lee *et al.* reported graphic data indicating about 37% and 26% for kVp values equivalent to those used in this work. The differences might be explained based on the fact that Lee *et al.* used a 24.5 mm Al filtration at all kVps, and reference values for the DQE based on an ideal counting detector. With respect to the MTF, others have reported relationships closely following that for an ideal square pixel that collects all of the charge created for x-ray absorptions occurring in the nominal pixel area. For such an ideal device, the ideal MTF is given by $\mathrm{sinc}_{\pi}(pf)$, where p is the pixel size in mm and f is the spatial frequency in mm^{-1}. In this work, we observed a deviation of the measured MTF relative to the ideal MTF with the ratio falling from 1.0 to 0.87 as the frequency increased from zero to 1.5 mm^{-1}. Between a frequency of 1.5 mm^{-1} and the limiting frequency of 3.6 mm^{-1}, the ratio remained constant at about 0.87. Using an x-ray Monte Carlo analysis for a detector with the same a-Se thickness, we found very similar behavior with an MTF reduction of 0.87 to 0.88 when the substrate glass is taken to be Corning 7059.[22] This type of glass is often used for electronic devices and produces fluorescent x-rays that are the cause of the MTF reduction. Similar observations have been made for an indirect detector by Yorkston *et al.*[23]

Our results for the XQ/i system are also in general agreement with previous reports.[7,8,24] For the estimation of the presampled MTF, Granfors and Aufrichtig used an edge method, while Floyd *et al.* used a slit technique. An MTF of 0.22 at the limiting frequency of 2.5 mm^{-1} reported in this work is comparable to but slightly lower than the values reported by those investigators, 0.26 and 0.24, respectively. The slight discrepancies between the MTF results of the three studies may be attributed the detector-to-detector variations, as three different physical devices were tested in the three studies, and to the differences in the measurement methods. Using comparable exposures, the extrapolated DQE values for the XQ/i system at zero frequency were also similar; 66% in all three studies. However, at 2.5 mm^{-1}, the DQEs were somewhat different: 20% and 15% in the diagonal and axial directions in our study, 24% by Granfors and Aufrichtig and 27% by Floyd *et al.* There are notable differences between these studies that might have a bearing in understanding the differences and resolving the discrepancies. They are as follows:

(1) Beam quality differences: RQA5 was used for both this work and that of Granfors and Aufrichtig, whereas Floyd *et al.* used 70 kVp with 0.5 mm Cu. Based on a com-

puter simulation by xSpect, assuming a nominal 500 micron thickness of CsI, the DQE for a 70kVp/0.5 mm Cu beam is ~3% higher than that for a 74 kVp/RQA5 beam.

(2) Counting versus energy integrating ideal detectors: The previous two studies assumed the ideal detector as a photon counting detector whereas this study assumed the ideal detector as an energy integrating detector. There are thus differences in the ideal SNR^2 used in the studies, not all of which can be explained by differences in the definition of the ideal detector. The values used for the ideal SNR^2 per mR were $280\,000\ mm^{-2}\,mR^{-1}$ in Granfors and Aufrichtig, $271\,500\ mm^{-2}\,mR^{-1}$ in Floyd *et al.*, and $255\,855\ mm^{-2}\,mR^{-1}$ in this study. This difference increases our RQA5 DQEs by 9.4% relative to Granfors' DQE. For the Floyd *et al.* results, the use of a slightly different technique also influences the ideal SNR^2. Assuming a nominal intrinsic filtration of 2.6 mm Al, a simulation by xSpect predicts an ideal counting SNR^2/mR of $250\,970\ mm^{-2}\,mR^{-1}$ for a 70 kVp/0.5 mm Cu as opposed to 271 500 used by Floyd *et al.* (4.9% difference) or 263 180 predicted for RQA5 (see Table II).

(3) Detector secondary layers: Granfors and Aufrichtig evaluated a detector with no secondary barriers except for a protective seal. The system tested by Floyd *et al.* included the detector cover plate (~9.0% and ~5.1% attenuation at RQA5 and RQA9, respectively) and an automatic exposure control (AEC) ionization chamber (~2.8% and ~1.3% attenuation at RQA5 and RQA9, respectively). Our system included the AEC assembly, but not the cover plate. Accounting for the attenuation layer will increase our DQEs with respect to Granfors' by 2.8% and decrease them with respect to Floyd's by 9.0% at all frequencies. Similarly, the Floyd *et al.* results should be increased by 12% to be compared against Granfors'.

(4) MTF differences: The slight differences in the measured MTFs, especially at high spatial frequencies, have a squared effect on the resultant DQE. Compared to Granfors', the 0.04 MTF difference at the Nyquist frequency, where we measured an MTF of 0.22, translates to 40% difference in DQE. Compared to Floyds', the corresponding 0.02 MTF difference translates to 19% difference in DQE. Floyd *et al.* also used expectation MTF (EMTF) for the DQE assessment as opposed to the presampled MTF in the other two studies. That alone would have a direct effect in increasing their reported DQE at high spatial frequencies, approaching 67% at $2.5\ mm^{-1}$.

(5) 2D NPS to 1D NPS transformation: Different methods have been used to extract a 1D NPS from the 2D NPS in order to estimate the DQE. Granfors and Aufrichtig used radial averaging, Floyd *et al.* used axial-band averaging, while this study used the axial as well as a new diagonal-band averaging method. At low frequencies, the three methods generate equivalent NPS and thus DQE, as illustrated in Fig. 8. However, at high frequencies, the DQE is highest for the diagonal method followed by that of the radial method and the axial method. The difference can be explained on the basis of reduced noise aliasing in the off-axes directions. Figure 8 also demonstrates how the width of the frequency band averaged to obtain the 1D NPS affects the resulting DQE. In general, the DQE is higher for wider bands and for the bands that exclude the central axial axes. For the XQ/i system, depending on the exact method to deduce the 1D NPS, the resulting DQE can vary by up to 0.05 (8%) and 0.07 (48%) at low and high frequencies.

(6) Dosimeter calibration: All methods estimated the ideal SNR^2 by experimentally measuring the exposure. Variations in the response of different dosimeter devices of up to 5% must always be recognized.

The above comparisons demonstrate the complexities in comparing performance measurements from different laboratories that might use slightly different methodologies to assess the DQE of digital radiographic systems. Direct comparison of values from different studies is thus not straightforward and should take into account the nuances of the assessment methodologies. Most valid comparisons of the performance of digital radiographic system may only be made by investigations in which identical assessment methods are applied.

Amongst the three systems, certain differences are best understood by considering the product of the exposure and the NPS determined in the diagonal direction as shown in Fig. 9. For systems whose noise is due only to statistical fluctuations associated with the detection of a limited number of quanta, the exposure normalized NPS curves vary little as a function of exposure, as seen for the DRC and XQ/i systems. The results for the DiDi system demonstrated significant change with exposure due to added instrumentation noise and applied preprocessing filters. Generally, the relative noise increased with exposure. This causes a reduction in DQE with increasing exposure (not shown). However, it should be pointed out that the DQE at high exposures may have a relatively less clinical importance compared to that at lower exposures in that the noise equivalent quanta (NEQ) is high enough so that the additional noise may be inconsequential. Furthermore, for this particular system, the tested exposure levels were beyond the targeted exposure level for the system (0.285 mR, 2.5 uGy, 400 speed). At low exposures, where the instrumentation noise for the DiDi system was not noticeable, the exposure-normalized NPS exhibited relative elevation at intermediate frequencies when compared to the XQ/i system. This is likely due to the effects of the enhancement filter that also increases the MTF of the DiDi relative to the XQ/i (see Fig. 3).

For this study, we used a new edge device for evaluating the MTF. Compared to our previous edge test device, the new device is thinner which makes it easier to align, and is made of a more rigid material (i.e., Pt–Ir alloy) which makes it more durable. The overall shape of the device is square and all four edges have been polished so that horizontal and vertical MTF can be estimated from one exposure. The atomic number of this device ($Z=\sim 78$) is lower than that for the lead edge that we have previously used ($Z=82$)[13] with a

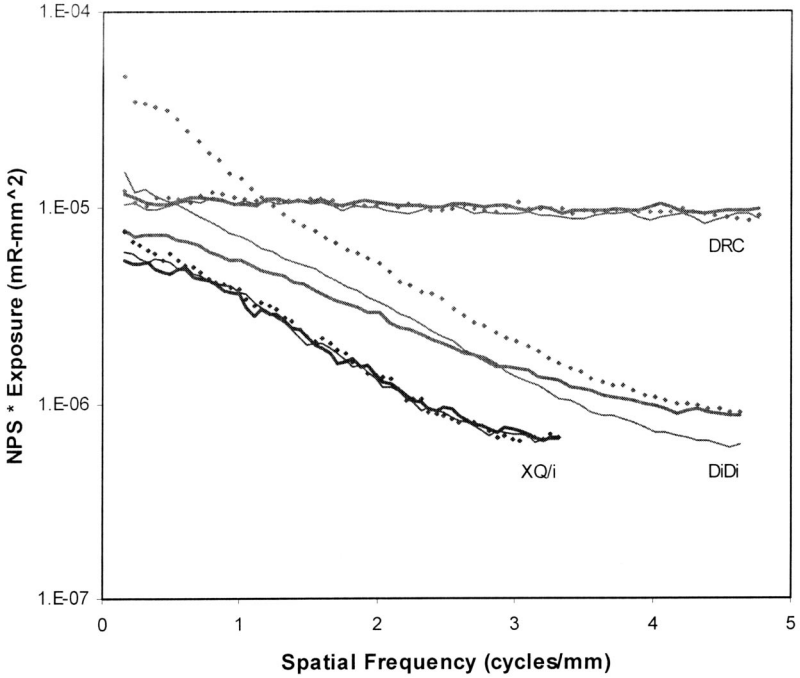

FIG. 9. The measured product of exposure and the NPS in the 45° diagonal direction for the DRC, XQ/i, and DiDi systems at a low exposure level (—) (0.38, 0.27, and 0.26 mR, respectively), medium exposure level (–) (1.74, 1.19, and 1.23 mR, respectively), and high exposure level (— — —) (6.88, 4.9, and 5.16 mR, respectively). The data were acquired with the RQA5 beam quality.

correspondingly lower *k*-electron binding energy (78.4 compared to 88.0 keV). For the RQA5 technique, no fluorescent radiation is emitted from either of the edge devices. For the RQA9 technique using either edge device, we have observed low frequency variations in the acquired signal that may be due to fluorescent radiation emitted by the test device. Further work is required to identify a geometry and an edge material that will minimize the influence of fluorescent radiation on the measured edge spread function at high energies. Additionally, in this work, new software was employed to deduce the MTF from the image of the edge test device. Using the same system and the same measurement geometry, we have verified that the new test device and the new software provide results comparable to our previous methods,[13] as illustrated in Fig. 10.

V. CONCLUSIONS

A comparison of the physical performance characteristics of a direct and two indirect digital radiography detectors demonstrated differences that were consistent with the different methods used to convert absorbed x-ray to electronic

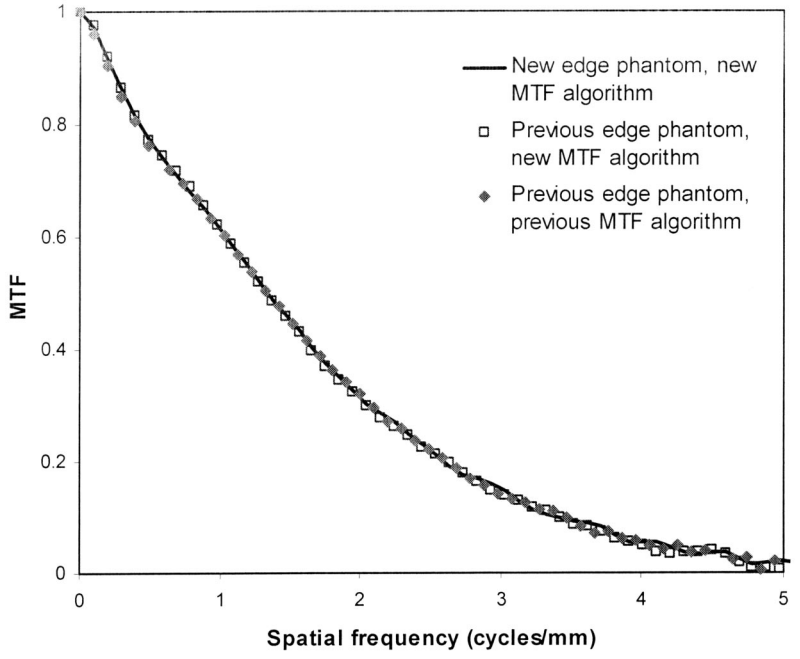

FIG. 10. The comparison of MTF measurements made with previous and new version of the MTF analysis algorithm (lines 1 and 2), and between the previous and new edge test device (lines 1 and 3). The results are nearly identical with $R^2 > 0.9997$.

charge. The MTF of the direct detection system differs slightly from the ideal function due to the effects of fluorescent radiation transport in the device. The indirect detection systems demonstrate a reduction in MTF consistent with the expected light spread within the device. The direct detection system has a flat noise power spectrum indicating little noise correlation from one pixel to another. The indirect detection systems demonstrate diminished noise power at high spatial frequencies consistent with the effects of light spread. The DQE for the direct system demonstrates a nearly linear decrease with frequency. In comparison, the DQE of the indirect detection systems is seen to decrease more rapidly at high frequencies. Overall, the high absorption of the indirect detection system provides better performance below a spatial frequency of approximately $2.5\,\mathrm{mm}^{-1}$, while the negligible blur, smaller Lubbert's effect, and the small pixel size of the direct detection system provides better performance above that frequency. The DQE and the overall conclusions above cannot be readily drawn from the second indirect system tested (the Philips Digital Diagnost System) due to the preprocessing applied to the raw image data from that system.

The actual clinical performance of the various systems depends on many factors other than DQE, including the operating exposure ranges for the acquisition of clinical images, detector sensitivity to scattered radiation, the use of antiscatter grids, and image processing. Nevertheless, assuming similar patient exposures, some general implications can be drawn from the comparison of the results on the two particular direct and indirect digital radiography systems that were tested in this study (i.e., DRC and XQ/i). The high MTF and superior DQE of the direct system above approximately $2.5\,\mathrm{mm}^{-1}$ suggest that this system may be particularly effective in radiographic applications where fine anatomic structures need to be imaged with high detail and contrast. Utilization of this system for imaging trabecular bone structures in skeletal extremities, for example, would thus be indicated. On the other hand, the extremely high DQE of the indirect system at frequencies below $2.5\,\mathrm{mm}^{-1}$ makes it attractive in radiographic applications where the visibility of low contrast anatomic structures is limited by noise. Utilization of these systems for imaging of lung nodules in thoracic imaging, for example, would thus be indicated. Notwithstanding these conclusions are the relative significance of high and low frequencies for particular clinical tasks, and clinical implications of signal and noise aliasing in the direct systems, both of which await further investigations.

ACKNOWLEDGMENTS

The authors gratefully acknowledge James T. Dobbin III and Harrell G. Chotas of Duke University for helpful discussions and valuable contributions to this study. The authors also wish to thank Ulrich Neitzel of Phillips Medical Systems, Denny Lee, Brian Rodrick, and Greg Powell of Direct Radiography Corp., and Carson Thomas, Paul Granfors, Ken Kump, Scott Schubert, and Ping Xue of GE for their assistance with this study.

[a]Electronic mail: samei@duke.edu

[1] M. J. Yaffee and J. A. Rowlands, "X-ray detectors for digital radiography," Phys. Med. Biol. **42**, 1–39 (1997).
[2] D. L. Lee, L. K. Cheung, B. G. Rodricks, and G. F. Powell, "Improved imaging performance of a 14×17-inch digital radiography system using Se/TFT detector," Proc. SPIE **3336**, 14–23 (1998).
[3] W. Zhao, I. Blevis, S. Germann, J. A. Rowlands, D. Waechter, and Z. Huang, "Digital radiology using active matrix readout of amorphous selenium: Construction and evaluation of a prototype real-time detector," Med. Phys. **24**, 1834–1843 (1997).
[4] J. H. Siewerdsen, L. E. Antonuk, Y. El-Mohri, J. Yorkston, W. Huang, J. M. Boudry, and I. A. Cunningham, "Empirical and theoretical investigation of the noise performance of indirect detection, active matrix flat-panel imagers (AMFPIs) for diagnostic radiology," Med. Phys. **24**, 71–89 (1997).
[5] C. Chaussat, J. Chabbal, T. Ducourant, V. Spinnler, G. Vieux, and R. Neyret, "New CsI/*a*-Si 17″×17″ x-ray flat-panel detector provides superior detectivity and immediate direct digital output for general radiography systems," Proc. SPIE **3336**, 45–56 (1998).
[6] R. E. Colbeth, V. N. Cooper, D. L. Gilblom, R. A. Harris, I. D. Job, M. E. Klausmeier-Brown, M. Marc, J. M. Pavkovich, E. J. Seppi, E. G. Shapiro, M. D. Wright, and J. M. Yu, "Characterization of a third-generation multimode sensor panel," Proc. SPIE **3659**, 491–500 (1999).
[7] P. R. Granfors and R. Aufrichtig, "Performance of a 41 cm×41 cm amorphous silicon flat panel x-ray detector for radiographic imaging applications," Med. Phys. **27**, 1324–1331 (2000).
[8] C. E. Floyd, Jr., R. J. Warp, J. T. Dobbins III, H. G. Chotas, A. H. Baydush, R. Vargas-Voracek, and C. E. Ravin, "Imaging characteristics of an amorphous silicon flat-panel detector for digital chest radiography," Radiology **218**, 683–688 (2001).
[9] J. H. Launders, S. M. Kengyelics, and A. R. Cowen, "A comprehensive physical image quality evaluation of a selenium based digital x-ray imaging system for thorax radiography," Med. Phys. **25**, 986–997 (1998).
[10] E. L. Gingold, D. L. Lee, L. S. Jeromin, B. G. Rodricks, M. G. Hoffberg, and C.L. Williams, "Development of a novel high-resolution direct conversion x-ray detector," Proc. SPIE **3977**, 185–193 (2000).
[11] E. Samei, M. J. Flynn, H. G. Chotas, and J. T. Dobbins III, "DQE of direct and indirect digital radiographic systems," Proc. SPIE **4320**, 189–197 (2001).
[12] IEC 1267, *Medical Diagnostic X-ray Equipment—Radiation Conditions for Use in the Determination of Characteristics*, 1st ed. (IEC, Geneva, Switzerland, 1994).
[13] E. Samei, M. J. Flynn, and D. A. Reimann, "A method for measuring the presampled MTF of digital radiographic systems using an edge test device," Med. Phys. **25**, 102–113 (1998).
[14] K. A. Fetterly and N. J. Hangiandreou, "Image quality evaluation of a desktop computed radiography system," Med. Phys. **27**, 2669–2679 (2000).
[15] W. H. Press, S. A. Teukolsky, W. T. Vetterling, and B. P. Flannery, *Numerical Recipes in C, The Art of Scientific Computing*, 2nd ed. (Cambridge University Press, Cambridge, 1992), pp. 650–655.
[16] W. K. Pratt, *Digital Image Processing* (Wiley, New York, 1991).
[17] M. J. Flynn and E. Samei, "Experimental comparison of noise and resolution for 2k and 4k storage phosphor radiography systems," Med. Phys. **26**, 1612–1623 (1999).
[18] E. Samei and M. J. Flynn, "An experimental comparison of detector performance for computed radiography systems," Med. Phys. **29**, 447–459 (2002).
[19] D. Hoeschen, "DQE of digital x-ray imaging systems: a challenge for standardization," Proc. SPIE **4320**, 280–286 (2001).
[20] K. A. Fetterly, N. J. Hangiandreou, B. A. Schueler, and E. R. Ritenour, "Measurement of the presampled two-dimensional modulation transfer function of digital imaging systems," Med. Phys. **29**, 913–921 (2002).
[21] S. M. Kengyelics, A. R. Cowen, and A. G. Davies, "Image quality evaluation of a direct digital radiography detector operating in a UK radiology department," Proc. SPIE **3659**, 24–35 (1999).

[22] M. J. Flynn, S. Wilderman, and J. Kanicki, ''Effect of secondary radiations on the performance of digital radiographic detectors,'' Proc. SPIE **3336**, 326–336 (1998).
[23] J. Yorkston, L. E. Antonuk, Y. El-Mohri, K. -W. Jee, W. Huang, M. Maolinbay, X. Rong, J. H. Siewerdsen, and D. P. Truernicht, ''Improved spatial resolution in flat panel imaging systems,'' Proc. SPIE **3336**, 556–563 (1998).
[24] P. R. Granfors and R. Aufrichtig, ''DQE(f) of an amorphous-silicon flat-panel x-ray detector: detector parameter influences and measurement methodology,'' Proc. SPIE **3977**, 2–13 (2000).